All-Silicon Active and Passive Guided-Wave Components for $\lambda = 1.3$ and $1.6\ \mu m$

RICHARD A. SOREF, SENIOR MEMBER, IEEE, AND JOSEPH P. LORENZO

***Abstract*—End-coupled planar and channel waveguides at 1.3 μm have been demonstrated in single-crystal Si layers grown epitaxially on heavily doped Si substrates, and an optical power divider consisting of intersecting channels was designed and fabricated. Optical switches in Si based on electrooptic, acoustooptic, and optical-injection mechanisms are described. The advantages of all-silicon integrated optical components are discussed.**

I. Introduction

FOR the past ten years, oxidized silicon has served as a substrate for Ta_2O_5, ZnO, Si_3N_4, and other waveguide materials (see, for example, [1]). However, optical waveguiding in silicon *per se* has not been explored, apart from some work at $\lambda = 10.6\ \mu m$ [2]–[4]. Because of its transparency (Section II below), single-crystal silicon is suitable for low-loss waveguiding at the fiber-optical communications wavelengths $\lambda = 1.3$ and $1.55\ \mu m$.

Silicon is a "new" material in the context of integrated optics even though Si is the most thoroughly studied semiconductor in the world. There is reason to believe that Si can serve as the medium for a variety of guided-wave optical components in much the same manner as III–V semiconductor compounds, while at the same time avoiding the inherent complexities of binary, ternary, and quaternary alloys.

We have embarked on a research-and-development program to determine the suitability of Si for 1.3/1.6 μm integrated optics. The goals of the program are to develop appropriate crystal-layering techniques for waveguiding, to construct passive waveguide devices, to investigate techniques for minimizing propagation loss, to build active guided-wave devices including electrooptical switches, and to build waveguide-integrated photodetectors. Early results are reported in this paper. So far, the results are encouraging, but much of the research lies ahead of us.

The project was motivated by two considerations: 1) many of the processes developed for the Si electronic circuit industry can be applied to Si optical devices, and 2) high-speed Si electronic circuits can be combined monolithically with Si guided-wave devices in an optoelectronic integration.

The organization of this paper is as follows: Section II reviews the properties of Si pertaining to guiding, Section III describes Si waveguide structures, Section IV presents designs for Si electrooptical switches and reviews other switching mechanisms, and Section V presents the experimental results to date.

Manuscript received September 5, 1985; revised January 14, 1986.

The authors are with the Solid State Sciences Division, Rome Air Development Center, Hanscom Air Force Base, MA 01731.

IEEE Log Number 8608108.

II. Infrared Transmission

The transmission of Si at wavelengths beyond the band edge is governed by residual absorption and scattering losses. If the Si has residual impurities or is doped deliberately to provide electrically active impurities, free carriers will be present at room temperature. According to classical dispersion theory, those carriers will alter the real and imaginary parts of the Si dielectric constant. In optical terms, we say that the refraction and absorption indexes are changed by amounts Δn and $\Delta\alpha$, respectively. The analysis of Moss [5, eq. (2.33)] and Lubberts [6, eq. (23)] generalized for two carriers shows that

$$\Delta\alpha = (q^3\lambda^2/4\pi^2c^3n\epsilon_0) \cdot [N_e/m_{ce}^{*2}\mu_e + N_h/m_{ch}^{*2}\mu_h] \quad (1)$$

$$\Delta n = -(q^2\lambda^2/8\pi^2c^2n\epsilon_0) \cdot [N_e/m_{ce}^* + N_h/m_{ch}^*] \quad (2)$$

where q is the electronic charge, λ is the optical wavelength, n is the refractive index of pure Si, ϵ_0 is the permittivity of free space, N_e is the free electron concentration, N_h is the free hole concentration, m_{ce}^* is the conductivity effective mass of electrons (m_{ch}^* for holes), μ_e is the electron mobility, and μ_h is the hole mobility. The mobility data presented in Fig. 18 of Sze [7] and in Figs. 2–5 of Gise and Blanchard [8] show that μ_e decreases in a nonlinear fashion with increasing donor concentration, going from 1500 $cm^2/V \cdot s$ at $N_D = 10^{14}\ cm^{-3}$ down to 90 $cm^2/V \cdot s$ at 10^{20} donors/cm^3, while a similar decrease occurs for μ_h, with μ_h falling from 470 $cm^2/V \cdot s$ at 10^{14} acceptors/cm^3 to 45 $cm^2/V \cdot s$ at $N_A = 10^{20}\ cm^{-3}$.

The optical properties of Si were first studied more than 30 years ago, and the absorption band edge was well delineated by the measurements of Fan *et al.* [9]. However, in the near infrared, for $\lambda > \lambda_g$, there is very little data in the literature about the background or residual absorption in Si. This deficiency was remedied recently by the work of Swimm [10] who performed calorimetric measurements of α on a single-crystal Si sample whose resis-

0018-9197/86/0600-0873$01.00 © 1986 IEEE

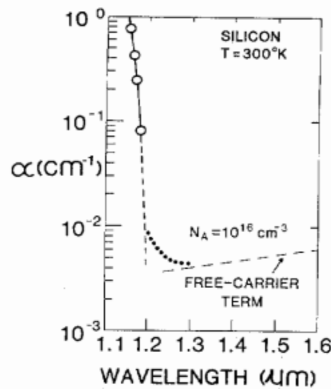

Fig. 1. Wavelength dependence of optical absorption for high-resistivity single-crystal Si from [9] and from our calculation of free-carrier absorption.

tivity was 10^4 Ω · cm and whose minority carrier lifetime was 5 ms. He found that $\alpha = 10^{-3}$ cm^{-1} at $\lambda = 1.32$ μm, a very low loss. Since samples like this are unusual, we calculated the free-carrier absorption over the 1.2–1.6 μm spectral range in a more commonplace sample, a p-type crystal containing 10^{16} impurities/cm^3. Neglecting the electron term in (1) and taking $n = 3.50$ and $m_{ch}^* = 0.39$ m_0 [5], we find from (1) the result plotted in Fig. 1. This figure also shows Fan's data. The inference drawn from Fig. 1 is that the materials loss in silicon waveguides will be very low (an inherent loss estimated to be much less than 1 dB/cm).

Continuing our quest for "new" materials systems, if we also consider the alloy system of Ge and Si, specifically Si-rich alloy crystals, we will obtain infrared transmission spectra for those materials that are very similar to that of Fig. 1, except that the band edge will be shifted to longer wavelengths. In the transparent region, the Ge-Si loss coefficients are expected to be as low as those of Si. Under the constraint that the material should be highly transmissive at 1.3 μm, we conclude that Ge–Si alloys are suitable for waveguiding when the mole fraction of Ge is 15 percent or less [11].

Returning to an analysis of pure Si, we note that scattering losses are negligible in bulk crystals, but if a waveguiding layer contains grain boundaries, twinning, lattice defects, etc., the scattering losses go up dramatically. It is suprising how large an effect the crystallinity has upon propagation loss at $\lambda = 1.3$ μm. To be specific, the absorption coefficient for undoped polycrystalline Si is 600 cm^{-1} at 1.3 μm (Jones [12]), while for amorphous undoped Si, $\alpha(1.3\ \mu m) = 3300$ cm^{-1} (Celler [13]). Similar behavior for films of silicon-on-sapphire and silicon-on-spinel was reported in a 1974 paper by Kuhl [14]. These results imply that poly-Si and amorphous-Si are far less desirable for waveguiding than single-crystal Si.

III. Waveguide Structures and Fabrication

Planar waveguiding takes place in a layer whose index of refraction is higher than that of adjacent layers. In silicon, there are several techniques that can be used to create layered structures with the required index "discontinuties." These techniques include, but are not limited to, epitaxial silicon-on-insulator (SOI) technology, ion implantation to form a low-index buried layer, and epitaxial growth of silicon on silicon. The resulting layered structures can be transformed by wet or dry etching into the desired geometry for three-dimensional channel waveguiding. Stress-induced index changes provide another means for making channel waveguides [15]. One can start with bulk material and deposit dielectric or metal strips to produce the desired tensile or compressive stresses.

Although we do not intend to describe each approach here, some brief comments come to mind. The all-silicon epi approach does produce high-quality waveguides, but the silicon-on-sapphire technique yields waveguides with relatively high propagation losses, most likely as a result of Si/Al_2O_3 interface scattering that arises from the lattice mismatch. The Si/Si epi approach has the added advantage of "leveraging" commercial circuit technology, that is, the Si/Si wafers that have been developed for the electronic circuit industry (CMOS–VLSI and discrete devices) will perform well in the optical guided-wave application. We have drawn upon this commercial epi material.

High-resistivity epitaxy of single-crystal Si on heavily doped single-crystal Si substrates has provided our best guiding results to date. Due to the presence of free carriers, the bulk substrate doping decreases the substrate's index of refraction with respect to the index of the lightly doped epitaxial layer. If the concentration of impurities in the epi is less than 10^{16} cm^{-3}, the epi index will not differ significantly from that of intrinsic Si. With the aid of (2), we have calculated the refractive index difference $\Delta n = n(\text{epi}) - n(\text{sub})$ as a function of N where N is the substrate impurity concentration in either n^+ or p^+ material. It was assumed that N ranged over the practical values of 10^{18}–10^{20} cm^{-3}. In (2), we used the approximation that N_e (sub) $= N$ for n^+ material (or that N_h (sub) $= N$ for p^+ material). This approximation is valid since, to first order, the shallow donors (or acceptors) are fully ionized at room temperature. Hence, the free-carrier concentration is the same as the impurity concentration.

Fig. 2 presents the calculated Δn at two wavelengths. The number of optical modes trapped by epi layer (the numerical aperture) depends to a certain extent upon the cladding or "superstrate" applied atop the epi, but it can be said from the result of Fig. 2 that the 10^{-3}–10^{-1} index difference is sufficient to provide trapping of "high-angle" rays in the epi, i.e., the guiding is effective. Some of the optical energy trapped in the epi will "tail" evanescently into the substrate. This can give rise to cladding loss if the substrate is too heavily doped. In other words, there is a tradeoff between the NA of the guide (Δn) and the cladding loss. The absorption coefficient of the substrate is calculated in Section IV below.

IV. Optical Switch Design

The crystal lattice of Si is centrosymmetric; therefore, Si does not exhibit the linear electrooptic effect (the Pock-

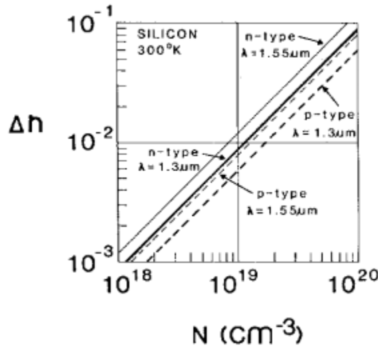

Fig. 2. Index-of-refraction difference, n(epi)-n(sub), versus substrate impurity concentration for epitaxial Si structure.

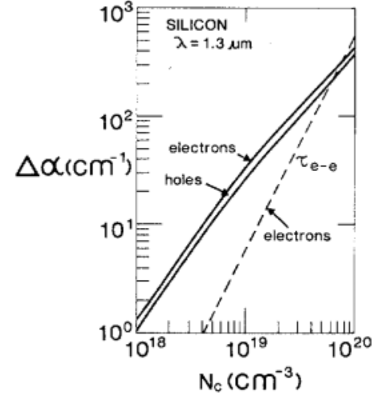

Fig. 3. Added optical absorption in Si due to the presence of N_c free carriers per cm^3.

els effect). For this reason, some people would argue that Si is not an active material, and is therefore not genuinely useful in integrated optics. We do not share this pessimistic view. On the contrary, there are several optical switching mechanisms that have the potential to provide active switching directly in silicon. Five such mechanisms are proposed and discussed in this section.

Starting with InGaAsP waveguides, Mikami and Nakagome [16] demonstrated 2×2 optical switching by injecting free carriers into the intersection region of crossed guides. The refractive index of the intersection was perturbed significantly ($\Delta n = 5 \times 10^{-3}$) at 10^{18} carriers/cm^3 due to the plasma dispersion effect, and electrical injection from a forward-biased p–n heterojunction was used. It is straightforward to apply these injection techniques to silicon; in fact, the technology is much more familiar in Si than in InP, and in Si one can use homojunctions rather than heterojunctions.

We have calculated the refractive index changes in Si that can be expected when a density N_e of electrons is injected into an Si waveguide. To do this, we use (2) with $\lambda = 1.3$ μm, $n = 3.50$, and $m_{ce}^* = 0.26$ m_0 [5]. We find that $\Delta n = 0.9 \times 10^{-3}$ when $N_e = 10^{18}$ cm^{-3}, a mode perturbation adequate for 2×2 electrooptical switching in the two-mode-interference device. As pointed out in [16], there is inevitably some loss associated with high levels of injected carriers. This is described by the Kramers–Kronig relations. We have calculated the optical absorption coefficient of the injection region $\Delta\alpha$ in cm^{-1} for $N_e = 10^{18}$–10^{20} cm^{-3} using (1) and the mobility curves cited in Section III above. A similar calculation for hole injection was made. The result is presented in Fig. 3 where the abscissa N_c represents the injected carrier concentration. The fractional transmission of the X-structure switch is exp $[-\Delta\alpha L]$ where L is the length of the interaction region. When the monomode channels cross at an angle of 4° or more, L can be kept below 100 μm. Thus, the $\Delta\alpha$ results in Fig. 3 do not pose a serious insertion-loss problem for $N_e \approx 10^{18}$ cm^{-3}. If we wish to determine the optical loss coefficient of the n$^+$ (or p$^+$) waveguide substrate material, then we can interpret the abscissa N_c in Fig. 3 as the impurity concentration in the substrate. This interpretation is valid for the reason cited above in Section III. Therefore, Fig. 3 also shows the substrate loss as a function of the n$^+$ or p$^+$ doping density.

The main limitation of the electrooptic injection switch is the speed of response, which is limited by the carrier lifetime. There are many carrier recombination mechanisms as described in the review paper of Celler [13], and these are dependent upon the carrier concentration. Taking the range of N_e shown in Fig. 3, we find that the slowest recombination process (the limiting factor in the switch) is Auger recombination, and this lifetime ranges from 10^{-10} to 10^{-6} s ($\tau \sim 1/N_e^2$). These switching rates would be useful in many applications. Faster response could be obtained by diffusing "lifetime killers" such as gold into the waveguide material.

Returning briefly to the loss analysis for the switch, it should be noted that the loss equation can be recast in terms of an overall relaxation time τ for the carriers (Pankove [17, eq. (3-25)]), namely, $\Delta\alpha = q^2\lambda^2 N_e / 4\pi^2 c^3 n \epsilon_0 m_{ce}^* \tau$ where $1/\tau = 1/\tau_1 + 1/\tau_2 + \cdots + 1/\tau_n$, and τ_1, τ_2, etc., are the various energy-relaxation times (electron–electron, electron–plasmon, etc.). To first order, we can say that $\Delta\alpha$ is dominated by the fastest relaxation mechanism (the shortest τ_i) over the concentration range of N_e. Hence, in the above equation, we use the 10^{-14}–10^{-12} s electron–electron collision time from Celler ([13], $\tau \sim 1/N_e$) and find the $\Delta\alpha$ result labeled with the τ_{ee} caption in Fig. 3 (which agrees with the other analysis at large N_e).

We have discussed electrical control of an Si guided-wave device, but it should be noted that optical control is possible (as in "optical logic"). Here, one would use creation of electron–hole pairs, with free carriers arising from the absorption of short-wavelength photons (a band-to-band absorption process). For example, an intense control beam of green light could be focused on the desired region of the waveguide (at normal incidence, for example). The control-beam wavelength would be chosen for nearly complete absorption across the ~ 5 μm transverse dimension of the guide. This would produce Δn of the same magnitude as in Fig. 2 as desired, and would yield optically controlled optical switching.

Returning to electrooptic effects, we should point out

that the quadratic EO effect or Kerr effect is present in Si [18]. However, this effect becomes significant only at high field strengths, and it is not clear that the Kerr coefficients are of a practical magnitude in Si because the Kerr effect at 1.3 μm has not been reported in the literature. On the other hand, experimental results have been given in [19] on the optical Kerr effect in Si, a nonlinear optical effect.

There is another electric-field, called "electrorefraction," that is likely to be more practical than the Kerr effect. Measurements of electrorefraction in GaAs and InP were made recently by van Eck *et al.* [20], and we have discussed electrorefraction in Si in an unpublished memorandum. This effect is related to the electroabsorption effect (Franz–Keldysh effect) by the *K–K* dispersion relations, and electrorefraction may be thought of as the "real part" of the electroreflectance effect, an effect that has been known in Si for more than 20 years.

As van Eck points out, it is important to choose the optical wavelength to be in close proximity to the band edge in order to enhance the electrorefraction effect. For example, the photon energy should be typically 0.025 eV less than the energy gap E_g. If we assume a fixed wavelength such as $\lambda = 1.3$ μm, then it would be necessary to "tailor" the band gap of the waveguide material to satisfy the $h\nu$-E_g "nearness" criterion. As we have mentioned above, this could be done by using a mixed crystal of Ge and Si, that is, an Si-rich alloy. The size of the effect in Si (or in Si–Ge) and the required field strengths are expected to be comparable to those found in [20], although the effect may be slightly smaller in Si than in InP because Si is an indirect-gap material. Judging from the results on Ge (Pankove [17, Fig. 18-4]), one could expect Δn of approximately 10^{-4} in Si. To produce the electric control fields, one would use a reverse-biased p–n junction or a depletion-mode MOS gate structure on the Si waveguide.

As a final note on optical switching in Si, let us consider acoustooptics. It has been known for many years that Si is capable of efficient acoustooptic Bragg diffraction (Carleton and Soref [21]). The A–O figure of merit M_2 is relatively large at $\lambda = 10.6$ μm and is expected to be at least 2× larger at $\lambda = 1.3$ μm. Use of the A–O mechanism is already well known in integrated optics, via surface acoustic waves for example, and recent work has shown that channelized 2 × 2 optical switching is feasible with an acoustooptic stimulus [22]. For all of the above reasons, we feel that A–O switching in Si would be a practical approach [23].

V. Experimental Work

A. Sample Preparation

Optical fibers, detectors, and lasers are most conveniently coupled to the waveguide ends (direct or butt coupling) without the use of prism couplers. For that reason, we investigated means of preparing optically flat ends on the Si waveguide samples. A scribe-and-break approach was tried, but was abandoned because the resulting cleavage planes were not smooth enough at the epitaxial location (they had a jagged, cliff-edge appearance). Instead, we developed mechanical polishing techniques that were successful for optical end coupling. To obtain sharp corners on the epi wafers, we first "potted" two dry-etched epi wafers (Section V-B, below) in epoxy, with the epi films facing each other. The parallel epi layers were in contact with a 40 μm film of Tracon-3103 epoxy. It was important to choose adhesive whose hardness matched that of Si (Mohs 7). This reduced chipping during polishing and promoted sharp edges on the wafer. The wafer sandwich was cut into dice, typically 0.7 × 4 × 2 mm in size, using a slow-speed diamond-wheel saw. The input and output ends of the sample were polished with a Buehler Fibrmet machine using (in succession) 1.0 and 0.3 μm alumina-impregnated polyester paper. The end polish was "good" in the sense that the scratches and edge chips were < 0.5 μm in size, adequate for optical coupling.

B. Slab and Channel Waveguides

Optical-quality Si epitaxial layers, n on n^+, p on p^+, n on p^+, p on n^+ (and double epi) are available from commercial vendors in a variety of epi film thicknesses, with a range of impurity dopings available in the substrate. The resistivity of the epi layer is usually 5 $\Omega \cdot$ cm or higher. The orientation of the wafer plane is either $\langle 100 \rangle$ or $\langle 111 \rangle$ and the epi is formed (for example) by thermal decomposition of silane. The initial experiments were with planar waveguides at $\lambda = 1.3$ μm. After dicing and polishing, the waveguide length was typically 2 mm. All of the guides described in this paper (both planar and channel) are multimode. In the future, we shall move to single-mode structures. We observed slab waveguiding in the six samples listed in Table I. A variety of conductivity types and doping levels gave good results. To find the density of donors (or acceptors) in the Table I samples, one can use the nonlinear relationship given in Fig. 21 of Sze [7] that relates resistivity to N_A or N_D. For example, the substrate donor concentration in sample 4 is 1.4–3.9 $\times 10^{19}$ cm^{-3}, while the epi donor density is 2.0×10^{14} cm^{-3}. The observed propagation losses in the planar guides of Table I ranged from 5 to 13 dB/cm. It is interesting to note that sample 6 had a highly multimode layer ($t = 43$ μm) which could be butt coupled to standard 50 μm D multimode fibers if the layer were milled into 50 μm wide channels.

The experimental setup consisted of a 1.32 μm InGaAsP laser diode with a 3 mW CW output, plus three microscope objectives, four Line Tool *x-y-z* micropositioners, and a sample stage that had two-axis rotation and tilt as well as *x-y-z* motion. Collimated light from the laser was focused by a 10× objective (0.25 NA in air) into the waveguide end, along the guide axis. The focal spot at the input surface had a diameter of approximately 4 μm. Using a 20× objective, a magnified image of light emerging from the waveguide (the near-field radiation pattern) was formed on an infrared vidicon. The rear surface of the guide was observed with an MII model 1500 camera that had a polished silicon filter at its input. The 1.3 μm

TABLE I
PARAMETERS OF SINGLE-CRYSTAL Si SLAB WAVEGUIDES

Sample Number	Conductivity	Dopants	Wafer Orientation	ρ(sub) ($\Omega \cdot$ cm)	ρ(epi) ($\Omega \cdot$ cm)	t(epi) (μm)
1	p/p^+	B	⟨100⟩	0.005–0.010	11.0	10.6
2	n/n^+	Sb	⟨100⟩	0.005–0.015	7.5	11.4
3	p/n^+	B/Sb	⟨100⟩	0.005–0.015	7.0	15.5
4	n/n^+	As	⟨111⟩	0.001–0.003	4.6	7.0
5	n/n^+	As	⟨100⟩	0.002–0.004	18.0	10.9
6	n/n^+	P/Sb	⟨100⟩	0.007–0.020	17.1	42.8

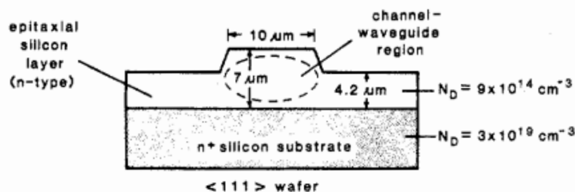

Fig. 4. Cross-section view of ridge waveguide.

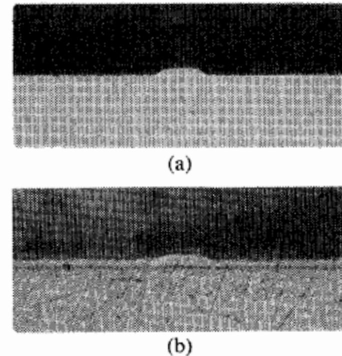

Fig. 5. Photomicrograph of (a) rib channel waveguide, (b) same waveguide etched with acid to reveal the epitaxial interface.

pattern was visualized with a 17 in TV monitor. For measurements of waveguide propagation loss, the vidicon was replaced with a 0.25 cm^2 area germanium photosensor that fed a digital optical power meter. The detector collected the entire cone of light emerging from the waveguide end. The optical output power of the waveguide was measured, and a reference transmission level (without the waveguide in place) was also measured. Corrections were made for the 1.6 dB Fresnel loss at each air/Si interface, that is, 3.2 dB were subtracted from the measured transmission loss.

The formation of channel guides was accomplished using photolithography on the epitaxial layer, followed by etching. One can use wet chemical etching (isotropic or preferential) or dry etching (plasma or ion beam). We utilized a plasma etch machine (with flourine chemistry) to produce flat sidewalls on the channels with minimal undercutting of the masking pattern.

The positive photoresist applied to the epi layer had stripe-shaped windows in the pattern, typically 10 μm wide. After depositing a 0.16 μm Ni–Au film on the resist, standard liftoff techniques were used, thereby leaving a pattern of Au stripes on the epi layer to serve as a mask for etching. After etching for 20 min at 300 W RF, approximately 2.8 μm of the epi layer was removed, but the region under the metal was not disturbed. The resulting channel waveguide, for a typical n/n^+ sample, is shown in the cross-sectional view of Fig. 4. This rib guide has walls that slope at about 40° to the vertical. The polished end of an actual ridge guide (photographed at 800× magnification) is shown in Fig. 5(a).

It is possible to delineate the interface between the epi layer and the substrate. This is done chemically with staining and decoration solutions. Fig. 5(b) is a cross-section photomicrograph (800×) of the selectively etched Si channel waveguide in which the epi boundary appears as a sharp line.

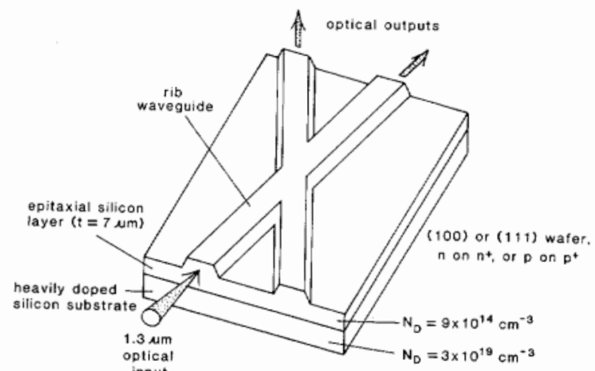

Fig. 6. Experimental optical power-divider structure.

C. Optical Power Divider

Over the long term, our goal is to build a 2 × 2 electrooptical switch with an intersecting-channel geometry (the so-called *X* structure). That device uses single-mode input and output waveguides with controlled two-mode interference in the intersection region. As a precursor of that device, we constructed multimode crossed-channel structures that serve as optical power dividers. These are monolithic, planar, integrated-optical structures in epitaxial silicon. The channel widths were 10, 15, and 20 μm, and the *X* patterns were 2 cm long. The crossing angle was 1.6, 2.2, or 2.8°. The rib height on the channels depended upon the etching time, and was approximately 3 μm. The test samples were 3 or 4 mm long.

Fig. 6 shows a perspective view of the power divider. Various splitting ratios were obtained as the crossing an-

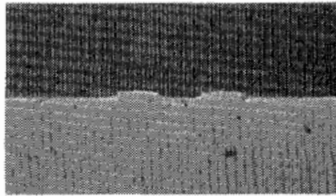

Fig. 7. Dual-channel output of experimental power-splitting device.

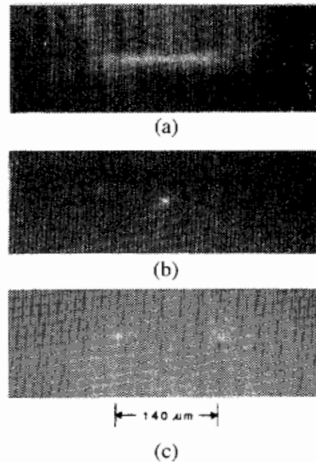

Fig. 8. Near-field 1.3 μm intensity patterns of (a) slab waveguide, sample 5, t = 10.9 μm, L = 2.0 mm; (b) channel waveguide, sample 4, t = 7 μm, L = 2.8 mm; (c) optical power divider, wafer 4, L = 3.0 mm. The scale is the same in all three photos.

gle, the ridge width, and the ridge height were changed. Fig. 7 is a photomicrograph (taken at 800× enlargement) of the polished output end of the optical power divider component. Fig. 8 presents a comparison of the optical performance of three Si waveguide components: a slab guide, a channel and a power divider. The optical near-field intensity pattern at 1.3 μm is shown for the three devices.

D. Discussion of Results

The present guides represent a "first effort" and were not optimized. The observed propagation loss at 1.3 μm ranged from 5 to 13 dB/cm in the slab guides and from 15 to 20 dB/cm in the rib channels. Considering the channels, the overall or observed loss includes absorption loss, scattering loss, radiation loss, and coupling loss. In the first category are material loss, metal loading loss, substrate loss, and superstrate loss (the last two from optical evanescent tailing). In the second category are channel wall-roughness loss and epi/substrate interface loss. The third category includes loss that occurs when the index difference is not large enough to confine the NA of the input beam completely or when the proportions of rib do not produce good mode confinement. The fourth category is the loss due to scratches, digs, and chips on the waveguide ends. Clearly, most of these loss contributions can be reduced significantly from their present values by further development of Si waveguide fabrication.

In tests with infrared polarizers, it was found that the Si planar waveguides supported both TE and TM modes in approximately equal numbers. This result is expected because silicon is a cubic, nonbirefringent material. In our epitaxial approach, both the guiding layer and the substrate are optically isotropic. Hence, the index difference in Fig. 2 is polarization independent: Δn(TE) = Δn(TM).

VI. Summary

Channel waveguiding and planar waveguiding at λ = 1.3 μm (with end-fire coupling) have been demonstrated in single-crystal silicon layers grown epitaxially on heavily doped Si substrates. A monolithic Si integrated-optical component (the first of its kind) has been built and tested. It was an optical power divider consisting of two intersecting channel waveguides. Active Si components were proposed. Five techniques for making 2×2 and $N \times N$ optical switches in Si are injection of free carriers by a forward-biased p–n junction, optical injection, the Kerr effect, electrorefraction using a reverse-biased contact, and acoustooptic Bragg diffraction.

Two advantages of Si guided-wave optical circuits are monolithic optoelectronic integration with high-speed Si electronic circuits [24] and utilization in optics of well-developed processing techniques from the electronics industry [25]. From the foregoing information, we infer that single-crystal Si will be suitable for building directional couplers, filters, star couplers, optical switches, mode converters, polarizers, interferometers, and modulators that operate at λ = 1.3 or 1.6 μm (and beyond)—essentially every integrated-optical component except an optical source [26]. The use of Si for photodetection at 1.3 μm has also been suggested [27].

Acknowledgment

The following people at RADC made important contributions to this project, and we wish to thank them for their help: C. E. Ludington, S. Spaziani, B. R. Bennett, A. C. Yang, and R. Payne. The laser diodes were kindly provided by J. N. Walpole and R. C. Williamson of M.I.T. Lincoln Laboratory, and important assistance on the generation of photomasks was given by B. Kosicki, G. Durant, and H. Pichler, also of M.I.T. Lincoln Laboratory. The wafers were supplied by Cincinnati Milacron Inc., Scientific Devices Inc.(SDI), and Spire Corporation.

References

[1] J. T. Boyd, R. W. Wu, D. E. Zelmon, A. Naumann, and H. A. Timlin, "Planar and channel optical waveguides utilizing silicon technology," in *Proc. 1st Int. Conf. Integrated Opt. Circuit Eng.*, SPIE vol. 517, 1984, pp. 100–105.
[2] M. Willander, "Carrier dependent parameters in a silicon optical waveguide," *J. Appl. Phys.*, vol. 54, p. 4660, 1983.
[3] ——, "Surface recombination velocity in a silicon optical waveguide," *Appl. Phys. A (Germany)*, vol. A31, p. 45, 1983.
[4] C. Falco, J. Botineau, A. Azema, M. deMicheli, and D. B. Ostrowsky, "Optical properties determination at 10.6 μm of thin semiconducting layers," *Appl. Phys. A (Germany)*, vol. A30, p. 23, 1983.
[5] T. S. Moss, *Optical Properties of Semi-Conductors*. London: Butterworths, 1959.
[6] G. Lubberts, B. C. Burkey, F. Moser, and E. A. Trabka, "Optical

properties of phosphorous-doped polycrystalline silicon layers," *J. Appl. Phys.*, vol. 52, p. 6870, 1981.
[7] S. M. Sze, *Physics of Semiconductor Devices*, 2nd ed. New York: Wiley, 1981.
[8] P. E. Gise and R. Blanchard, *Semiconductor and Integrated Circuit Fabrication*. Reston, 1979.
[9] H. Y. Fan, M. L. Shepherd, and W. Spitzer, "Infrared absorption and energy-band structure of germanium and silicon," in *Proc. Photoconductivity Conf.*, Atlantic City, NJ, Nov. 4, 1954, pp. 184–203.
[10] R. T. Swimm, "Optical absorption in the band gap of high-purity silicon," in *Dig. Papers, Conf. Basic Properties Opt. Mater.*, Gaithersburg, MD, May 7, 1985, pp. 158–159.
[11] It may be necessary to limit the Ge content to less than 5 percent in order to minimize strain in the Si–Ge crystal since the 5.65 Å lattice constant of Ge is larger than the 5.43 Å lattice parameter of Si.
[12] R. E. Jones and S. P. Wesolowski, "Electrical, thermoelectric, and optical properties of strongly degenerate polycrystalline silicon films," *J. Appl. Phys.*, vol. 56, p. 1701, 1984.
[13] G. K. Celler, "Modification of silicon properties with lasers, electron beams, and incoherent light," *Crit. Rev. Solid State Mater. Sci.*, vol. 12, issue 3, 1984.
[14] Ch. Kuhl, H. Schlotterer, and F. Schwidefsky, "Optical investigation of different silicon films," *J. Electrochem. Soc.*, vol. 121, pp. 1496–1500, 1974.
[15] D. J. Jackson and D. L. Persechini, "Waveguide formation in bulk GaAs and InP materials," *Electron. Lett.*, vol. 21, pp. 44–45, 1985.
[16] O. Mikami and H. Nakagome, "Waveguided optical switch in InGaAsP/InP using free-carrier plasma dispersion," *Electron. Lett.*, vol. 20, pp. 228–229, 1984.
[17] J. I. Pankove, *Optical Processes in Semiconductors*. Englewood Cliffs, NJ: Prentice-Hall, 1971.
[18] T. S. Narasimhamurty, *Photoelastic and Electro-Optic Properties of Crystals*. New York: Plenum, 1981.
[19] H. J. Eichler, "Optical multistability in silicon observed with a CW laser at 1.06 μm," *Opt. Commun.*, vol. 45, pp. 62–66, 1983.
[20] T. E. vanEck, L. M. Walpita, W. S. C. Chang, and H. H. Wieder, "Electrorefraction and electro-absorption in InP and GaAs near the band edge," in *Tech. Dig., CLEO 85*, Baltimore, MD, May 23, 1985, pp. 242–243, paper Th U5.
[21] H. R. Carleton and R. A. Soref, "Modulation of 10.6 μm laser radiation by ultrasonic diffraction," *Appl. Phys. Lett.*, vol. 9, pp. 110–112, 1966.
[22] C. T. Lee, "Optical gyroscope application of efficient crossed channel acoustooptic devices," *Appl. Phys. B (Germany)*, vol. B35, pp. 113–118, 1984.
[23] It should be noted that the surface acoustic waves (or bulk waves) would be launched into the Si by a thin-film transducer deposited on the Si (such as ZnO) because Si itself is not piezoelectric.
[24] Optoelectronic integration can also be obtained by growing III–V semiconductor structures on a silicon substrate. See, for example, the technical papers presented at Symp. A, "Heteroepitaxy on silicon," 1986 Spring Meet., Mater. Res. Soc., Palo Alto, CA, Apr. 15, 1986.
[25] Silicon wafers with 6 and 8 in diameters are available currently. These sizes offer considerable area for optoelectronic integration.
[26] Recent experimental work on electroluminescence in silicon suggests that Si LED's and LD's can be developed for 1.3–1.6 μm. Progress on Si optical sources is reported by H. Ennen, G. Pomrenke, A. Axman, K. Eisele, W. Haydl, and J. Schneider, "1.54 μm electroluminescence of erbium-doped silicon grown by molecular beam epitaxy," *Appl. Phys. Lett.*, vol. 46, pp. 381–383, 1985 and by T. G. Brown and D. G. Hall, "Observation of electroluminescence from excitons bound to isoelectronic impurities in crystalline silicon," *Appl. Phys. Lett.*, 1986, to be published.
[27] A. C. Yang, J. P. Lorenzo, and R. A. Soref, unpublished memo., 1985. The photodetection mechanism is internal photoelectric emission from a room-temperature Schottky-barrier contact placed on the side of a Si waveguide. The 1.3 μm light impinges at grazing incidence on the silicon/metal interface.

Richard A. Soref (S'58–M'63–SM'71) received the B.S.E.E. and M.S.E.E. degrees from the University of Wisconsin in 1958 and 1959, and the Ph.D. degree in electrical engineering from Stanford University, Stanford, CA, in 1963.

From 1963 to 1965, he worked in the optics and infrared group of M.I.T.'s Lincoln Laboratory, and in 1965, he joined the Technical Staff of the Sperry Research Center in Sudbury, MA, where he conducted research on a variety of topics including nonlinear optics, extrinsic Si infrared detectors, liquid crystal electrooptical devices, optical switching, and fiber-optic sensors. In November 1983, he joined Rome Air Development Center, Hanscom AFB, MA, as a Research Scientist in the Solid State Sciences Division. His current research interests include integrated optics and microwave applications of optics. He has authored or coauthored 65 journal articles and holds 14 patents.

Dr. Soref is a member of the American Physical Society the Society of Photo-Optical Instrumentation Engineers, and the Optical Society of America. He served as Chairman of the Boston Chapter IEEE Group on Electron Devices in 1969. He is currently an Editorial Advisor of *Optical Engineering*.

Joseph P. Lorenzo, photograph and biography not available at the time of publication.